



Implementation of the Community Radiative Transfer Model in Advanced Clear-Sky Processor for Oceans and validation against nighttime AVHRR radiances

Xing-Ming Liang,^{1,2} Alexander Ignatov,¹ and Yury Kihai^{1,3}

Received 8 August 2008; revised 4 January 2009; accepted 15 January 2009; published 25 March 2009.

[1] The fast Community Radiative Transfer Model (CRTM) has been integrated into National Environmental Satellite Data and Information Service's newly developed Advanced Clear-Sky Processor for Oceans (ACSPO). CRTM is used in conjunction with the National Centers for Environmental Prediction (NCEP) Global Forecast System atmospheric profiles and Reynolds weekly version 2 sea surface temperatures (SST) to simulate clear-sky brightness temperatures (BT). Model BTs are used to improve the ACSPO clear-sky mask, monitor quality of advanced very high resolution radiometer (AVHRR) BTs, and explore physical SST retrievals. This paper documents CRTM implementation in ACSPO version 1 and evaluates nighttime "model minus observation" (M-O) BT biases in three bands (3.7, 11, and 12 μm) of four AVHRR/3 instruments onboard NOAA-16, NOAA-17, NOAA-18, and MetOp-A. With careful treatment of input atmospheric and SST data, the agreement is generally good, showing only weak dependencies of M-O biases on view zenith angle, column water vapor, and wind speed. The agreement improves if Reynolds weekly SST is used instead of NCEP SST. Including surface reflection also reduces the M-O bias. After all optimizations, the M-O biases are within several tenths of a Kelvin. Consistency between different platforms is $\sim 0.1\text{K}$, except for NOAA-16 channel 3B, which is biased low compared to other platforms by $\sim 0.4\text{K}$. Our future plans include extending the analyses to daytime data and exploring physical SST retrievals. A web-based tool is being established to continuously monitor the M-O biases and physical SSTs. The validation methodology employed in this paper will be used to quantitatively measure the effect of each improvement on the M-O bias and physical SST.

Citation: Liang, X.-M., A. Ignatov, and Y. Kihai (2009), Implementation of the Community Radiative Transfer Model in Advanced Clear-Sky Processor for Oceans and validation against nighttime AVHRR radiances, *J. Geophys. Res.*, *114*, D06112, doi:10.1029/2008JD010960.

1. Introduction

[2] The new Advanced Clear-Sky Processor for Oceans (ACSPO) developed at NESDIS will replace the heritage Main Unit Task (MUT) system used since the early 1980s [McClain *et al.*, 1985; Walton *et al.*, 1998; Ignatov *et al.*, 2004]. Similar to the MUT, ACSPO generates AVHRR top-of-atmosphere (TOA) radiances over oceans, from which sea surface temperatures (SST) and aerosol products are derived. A major improvement in ACSPO over the MUT is the full integration of global clear-sky AVHRR radiances with the National Centers for Environmental Prediction Global Forecast System (NCEP/GFS) atmospheric and Reynolds *et al.* [2002] weekly version 2 SST fields. A fast Community

Radiative Transfer Model (CRTM) [Kleespies *et al.*, 2004; Han *et al.*, 2006], developed at the NESDIS Joint Center for Satellite Data Assimilation (JCSDA) and similar in its overall philosophy to the RTTOV (radiative transfer model for TOVS) [Saunders *et al.*, 1999, 2007], is then run with the GFS upper air and Reynolds SST input to predict TOA clear-sky brightness temperatures (BT) in AVHRR bands 3B (3.7 μm), 4 (11 μm), and 5 (12 μm). Currently, the CRTM BTs are used to perform quality control of AVHRR BTs and to improve the ACSPO clear-sky mask.

[3] Physical SST retrievals have been demonstrated to help improve SST retrieval [Merchant *et al.*, 1999, 2008; Merchant and Le Borgne, 2004] and are also being explored in ACSPO, in addition to the regression MultiChannel SST (MCSST) and Nonlinear SST (NLSST) retrievals preserved in ACSPO from the MUT. Accuracy of CRTM and global input fields is critically important for all these applications. Careful implementation of the forward CRTM in ACSPO, in conjunction with NCEP/GFS atmospheric and Reynolds SST data, and validation of CRTM BTs against AVHRR BTs are thus two major objectives of this study.

¹Center for Satellite Application and Research, NESDIS, NOAA, Camp Springs, Maryland, USA.

²Cooperative Institute for Research in the Atmospheres, Colorado State University, Fort Collins, Colorado, USA.

³QSS Group, Perot Systems Inc., Camp Springs, Maryland, USA.

[4] The paper is organized as follows. Section 2 briefly introduces the CRTM and describes the NCEP/GFS atmospheric and Reynolds SST data and their collocation with AVHRR observations. Section 3 describes satellite data used in this study. Section 4 documents the implementation of CRTM in ACSPO and optimization through a number of sensitivity analyses toward minimization of the M-O bias. In particular, accurate treatment of finite GFS layers in CRTM and using reflective (rather than black) surface model improves the M-O statistics in all AVHRR bands and for all platforms. Using *Reynolds et al.*'s [2002] weekly v.2 SST (referred to herein as the "Reynolds SST") rather than NCEP GFS SST (referred below as the "NCEP SST") also improves the M-O bias. The latter improvement is most noticeable in the coastal areas. In section 5, geographical distribution of the M-O bias is analyzed and its stability checked over a period of 1 week. In section 6, the effect of ambient clear-sky environment on the M-O biases is quantified, and asymptotic values of confident clear-sky M-O biases are estimated. Section 7 summarizes the results of this study. We conclude that, overall, the CRTM is much faster and performs more accurately and uniformly than MODTRAN4.2, and it can be used to start exploring physical SST retrievals in ACSPO.

2. CRTM and NCEP/GFS Atmospheric and Reynolds SST Inputs

2.1. CRTM

[5] In the CRTM version used in ACSPO v.1, extraterrestrial radiation is neglected and effects of scattering in the atmosphere omitted. Quantitative analyses of the effect of solar reflection on global M-O biases in Ch3B, 4 and 5 are currently underway. All analyses in this study are thus limited to only nighttime data, when these assumptions are better met. The radiative transfer equation used in CRTM for wide-band sensors such as the AVHRR is written as follows:

$$\bar{R}(\theta) = \varepsilon(\theta)\bar{B}(T_s)\bar{\tau}(\theta) + \bar{L}^\uparrow(\theta) + (1 - \varepsilon(53^\circ))\bar{L}^\downarrow(53^\circ)\bar{\tau}(\theta). \quad (1)$$

Sea surface emissivity, $\varepsilon(\theta)$, is discussed in more detail in section 2.2 below. $\bar{R}(\theta)$ is TOA radiance at sensor level; θ is view zenith angle; T_s is SST; and $\bar{B}(T_s)$ is its Planck radiance. Atmospheric transmittance, $\bar{\tau}(\theta)$, and upwelling and downwelling radiances, $\bar{L}^\uparrow(\theta)$ and $\bar{L}^\downarrow(53^\circ)$, are calculated within the CRTM.

[6] Terms in equation (1) with the overbar sign (except for surface emissivity, which in CRTM is specified at the central wavelength) represent band average values, i.e., convolved with the respective sensor spectral response, $\Phi(\theta)$. The monochromatic form of the radiative transfer equation is used in any fast RTM, such as the RTTOV or CRTM, because line-by-line calculations are computationally unaffordable for real-time applications. Resulting errors in TOA BTs are deemed to be small [e.g., *Sherlock et al.*, 2003; *Wan and Dozier*, 1996].

[7] The cornerstone of the CRTM is fast calculation of atmospheric transmittances using the "compact OPTRAN," which is a more accurate and computationally efficient version of OPTRAN v.6 [McMillin *et al.*, 2006; *Han et al.*, 2006]. Coefficients in the compact OPTRAN have been derived against LBLRTM v.9.4 transmittances, which use

the MTCKD v.1.2 for water vapor continuum [Clough *et al.*, 2005] and HITRAN2000 with 2001 updates for lines [Rothman *et al.*, 2003]. The transmittance profiles are calculated within the CRTM and further integrated with the emissions of each layer to calculate the TOA upwelling and surface downwelling atmospheric radiances. Comparisons of broadband BTs calculated using CRTM, and exact integration of the LBLRTM, show the root-mean-square deviations are less than 0.1K in all AVHRR bands [Han *et al.*, 2006].

[8] ACSPO v.1 uses CRTM "rev577," which was released on 15 May 2007. CRTM release 1.1 is currently available (<ftp://ftp.emc.ncep.noaa.gov/jcsda/CRTM/>), and subsequent versions of ACSPO will be upgraded accordingly. However, there is no significant change in the spectroscopy within the infrared windows between the rev577 and release 1.1, so that all results of this study obtained with rev577 should be representative of release 1.1.

2.2. Surface Emissivity

[9] CRTM users can select one of the two default emissivity models included in the CRTM: black surface, $\varepsilon \equiv 1$, or wind speed-dependent emissivity of *Wu and Smith* [1997], ε_{WS} . In the current CRTM version, emissivity is specified at the central wavelength of a band. CRTM can be also run with a user-defined emissivity model, ε_U , such as the *Sherlock* [1999], *Masuda* [2006], or Fresnel's model tested by *Dash and Ignatov* [2008].

[10] The surface emission term in equation (1) is calculated from the angle-dependent emissivity (CRTM default or user chosen), whereas for calculation of the surface reflectance term, emissivity at a fixed 53° direction is used, in conjunction with the downwelling atmospheric radiance from the same direction. This formulation was preserved by the CRTM Team from their earlier work over land surface, which is customarily assumed to be Lambertian [Han *et al.*, 2006]. Over ocean, however, the downwelling direction should be specified in conjunction with the view direction [e.g., *Watts et al.*, 1996; *Sherlock*, 1999]. Also, compared to the monochromatic emissivity used in the current CRTM version, using band-average emissivity is more consistent with the band-average nature of the CRTM [e.g., *Wan and Dozier*, 1996; *Sherlock et al.*, 2003]. Work is underway with the CRTM team to reconcile these inconsistencies. Results will be reported elsewhere.

2.3. NCEP/GFS Data

[11] Input to CRTM constitutes atmospheric profiles of pressure, air temperature, geopotential height, relative humidity (RH), and ozone specified from the NCEP/GFS files (www.emc.ncep.noaa.gov/modelinfo/). Several surface variables are also reported in GFS, including surface and air temperatures and pressure, as well as u and v components of wind speed (from which the near-surface wind speed used in this study is calculated as $V = \sqrt{u^2 + v^2}$). GFS data are generated 4 times a day for different forecast times at 1° latitude-longitude spatial resolution at 26 levels of atmospheric pressure and temperature from 1000 to 10 mbar, at 20 levels of relative humidity (RH) from 1000 to 100 mbar, and at 6 levels of O_3 from 100 to 10 mbar. All of this information is used in ACSPO, where GFS fields are linearly interpolated in time to match AVHRR observation time, using two 12-h forecasts separated by 6 h. These time-interpolated

fields are then used to simulate CRTM BTs at 1° resolution, which in turn are interpolated in space to match the AVHRR pixel.

[12] CRTM input should be specified in atmospheric layers, whereas GFS profiles are specified at levels, which bracket the corresponding layers. This level-to-layer conversion is left to CRTM users. Section 4.1 explores sensitivity to a particular implementation. In addition to H₂O and O₃, CRTM also accounts for the absorption due to five minor and uniformly mixed gases (CO₂, O₂, CO, CH₄, and N₂O) whose concentrations in the compact OPTRAN are set to globally nonvariable.

2.4. Reynolds Weekly v.2 SST

[13] Another input to CRTM is SST. The GFS files contain a “surface temperature” parameter, derived from the Reynolds weekly v.2 product over oceans and from land surface temperature over land. Although Reynolds and GFS SSTs are expected to be close, analyses in section 4 below show that the two SSTs differ. Further analyses show that Reynolds SST provides a more accurate input to CRTM, so it is, therefore, used in ACSPO v.1.

[14] Reynolds SST is bulk SST, and it does not resolve diurnal cycle. Also, during the nighttime, SST is cooler than daily average Reynolds SST. As a result, the global modeled BT (the “M”) used in this study may be biased warm by several tenths of a Kelvin [e.g., *Garand, 2003; Trigo and Viterbo, 2003*].

[15] During ACSPO development, however, *Reynolds et al. [2007]* daily SST has become available. This newer product is currently being tested to replace the weekly product, and results will be reported elsewhere.

3. Satellite Data Used in This Study

[16] In ACSPO products, CRTM BTs are reported side-by-side with AVHRR BTs derived from counts using the standard calibration, navigation, and quality-control information available on Level 1b files. The view and solar zenith angles, UTC, and latitude and longitude of the pixels are also saved in ACSPO from L1b data along with the derived ACSPO clear-sky mask [*Petrenko et al., 2008*].

[17] Data from four platforms are used in this study: NOAA-16, NOAA-17, NOAA-18, and MetOp-A. These satellites overpass at approximately 0430, 2130, 0200, and 2130 local time, respectively. As of the time of this writing, only NOAA-18 and MetOp-A satellites are operational at NESDIS, whereas NOAA-16 and NOAA-17 are kept in a back-up mode. Nevertheless, data from all four platforms are routinely processed and several case studies are used here.

[18] To minimize possible solar impingement on AVHRR blackbody, only nighttime data are used in this study. Nighttime pixels are defined as those with solar zenith angle > 118° [*Cao et al., 2001; Dash and Ignatov, 2008*]. In the case of NOAA-16, which currently flies close to the terminator, this condition may eliminate large areas in the high latitudes during the winter or spring seasons. However, we have opted to be on the “safe side” with the data screening to ensure high confidence in our validation results.

[19] In evaluating the results below, one should keep in mind that the AVHRR sensor on NOAA-16 has experienced continuous problems with scan motor. As a result, the quality

Table 1. Comparison of SVP Value Between the *Goff and Gratch [1946]* Approach and Polynomial Fit of Data From *Flatau et al. [1992]*

T (K)	<i>Flatau et al. [1992]</i> (hPa)	<i>Goff and Gratch [1946]</i> (hPa)	(F-G)/F (%)
188	5.21E-04	4.49E-04	13.7929
198	2.48E-03	2.30E-03	7.6028
208	1.00E-02	9.64E-03	3.9012
218	3.53E-02	3.46E-02	2.0725
228	0.1105	0.1092	1.1922
238	0.3108	0.3089	0.593
248	0.7975	0.7954	0.2603
258	1.8898	1.8867	0.1647
268	4.1718	4.1640	0.1859
278	8.6408	8.6224	0.2134
288	16.9019	16.8690	0.1948
298	31.4110	31.3700	0.1305
308	55.7698	55.7408	0.0519
318	95.0715	95.0689	0.0027

of its Level 1b data may be suboptimal during certain periods of time. Although all quality flags available on Level 1b data were applied in this study, the derived product may still be affected. We have chosen to keep NOAA-16 data in the analyses to see if they show any anomalies.

4. CRTM Implementation in ACSPO

[20] The way in which SST, atmospheric profiles, and modeled surface emissivity are specified in CRTM affects the simulated TOA BTs. This section discusses the CRTM implementation in ACSPO v.1 and options to minimize the M-O bias.

4.1. Treatment of Water Vapor in CRTM

[21] CRTM users need to convert GFS RH values reported at levels to the effective mass-mixing ratios of water vapor in layers. The mass-mixing ratio of water vapor, γ , is proportional to RH and to the saturation mixing ratio of water vapor as follows:

$$\gamma = \text{RH} \frac{MW_{\text{H}_2\text{O}}}{MW_{\text{dry}}} \frac{e_s(T)}{P - e_s(T)}. \quad (2)$$

Here, $MW_{\text{H}_2\text{O}}$ and MW_{dry} are molecular weights of water and dry air, respectively, P is atmospheric pressure, and $e_s(T)$ is saturation vapor pressure (SVP), which is a function of air temperature, T . Uncertainty in the layer γ may arise from the calculation of the SVP at levels, or from the way the level γ are converted to layer γ .

[22] In earlier SVP calculations, *Goff and Gratch's [1946]* empirical formulation was customarily used. Later, *Flatau et al. [1992]* fit a polynomial to the newer measurements by *Guildner et al. [1976]*. Table 1 compares the two SVP values for several air temperatures. The largest difference, up to 14%, takes place at low air temperatures. Since those are typically associated with low water vapor content, the effect on the TOA BTs is only 0.02K, globally. Nevertheless, the SVP formulation by Guildner and Flatau was adopted in ACSPO.

[23] Conversion of level γ to layer γ results in larger errors. In the initial ACSPO implementation (based on clouds from AVHRR extended, CLAVR-x (A. Heidinger, personal communication, 2006)), layer temperatures were first calculated

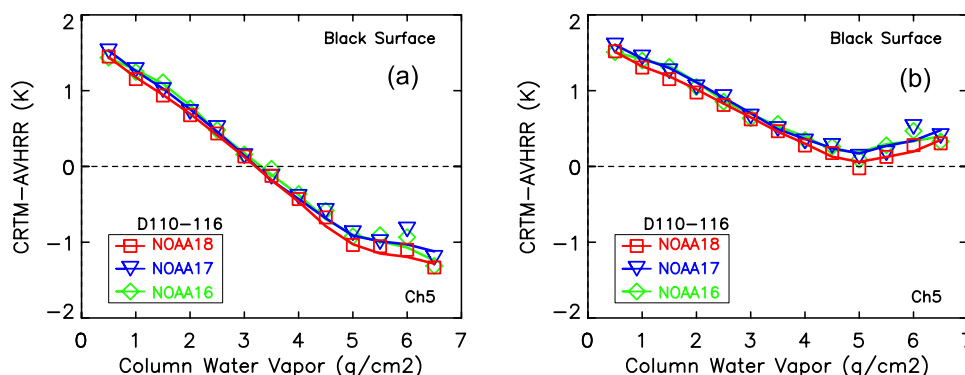


Figure 1. The mean M-O biases in AVHRR Ch5 onboard three NOAA platforms as a function of column water vapor for 1 week of global data from 20 to 26 April 2006. (a) Initial implementation and (b) corrected implementation. Data binned at $\Delta W = 0.5 \text{ g/cm}^2$.

as an average of the two levels' temperatures and used to calculate the SVP and subsequently the mass-mixing ratio in a layer using equation (2). Figure 1a shows an example of the M-O biases in Ch5 for 1 week of data in April 2006 and for three platforms (NOAA-16 through NOAA-18) using this initial implementation. The bias strongly depends upon column water vapor with amplitude of $\sim 3\text{K}$. A more appropriate approach is to first calculate the SVP and mass-mixing ratio at each level, and then calculate the layer's effective water vapor content, assuming its exponential decay with the height. Figure 1b shows that as a result, the M-O bias is reduced by a factor of 2 (from $\sim 3\text{K}$ to $\sim 1.5\text{K}$). This dramatic sensitivity is caused by the strong exponential dependence of the SVP on temperature shown in Table 1. A similar effect is also observed in Ch3b and Ch4, although of a smaller magnitude due to more transparent atmosphere here.

[24] We thus conclude that treatment of NCEP/GFS profiles in CRTM significantly affects the M-O bias and adopt the second approach in ACSPO. It is expected that for higher vertical resolution atmospheric profiles, such as the European Center for Medium-Range Weather Forecasting (ECMWF) data, RTM accuracy would be less sensitive to level-to-layer conversion uncertainty.

4.2. Downscaling 1° CRTM Calculations to AVHRR Pixel and New Cloud Mask in ACSPO

[25] Sensitivity analyses in Figure 1 were done with the initial code based on CLAVR-x. In ACSPO v.1, the clear-sky mask was improved [Petrenko *et al.*, 2008]. Also, an interpolation procedure was added to scale CRTM calculations performed in 1° GFS boxes down to 4-km or 1-km AVHRR pixel resolution. This procedure is based on expansion of modeled BTs into Taylor's array with respect to SST and slant path atmospheric optical depth and subsequent interpolation of the components of this simplified "Jacobian" in geographical coordinates.

[26] Figure 2a shows the M-O biases in AVHRR Ch5 for four platforms using ACSPO v.1 for 1 week in February 2007. Black surface model was used for consistency with Figure 1. Although the CRTM model remained unchanged from Figure 1, the pixel-level modeled BT ("M") has changed owing to the way the CRTM calculations performed at 1° resolution are now downscaled to AVHRR pixels. The AVHRR clear-sky radiances ("O") have also changed, owing

to the new ACSPO clear-sky mask. As a result, the dependence of the M-O bias in Figure 2a has further reduced from Figure 1b, especially at low ($W < 2 \text{ g cm}^{-2}$) and high ($W > 5 \text{ g cm}^{-2}$) water vapors. In the remaining part of this paper, ACSPO v.1 data are consistently used.

4.3. Surface Emissivity Model

[27] As expected, a different treatment of the GFS finite layers affects the M-O bias proportionately more toward higher water vapor contents. The low water vapor end remains unchanged and biased high by $\sim 1\text{K}$. A possible cause is the black surface assumption, which affects TOA BTs progressively larger toward more transparent atmospheres.

[28] Figure 2b replots the M-O biases from Figure 2a using the wind speed-dependent surface emissivity model by *Wu and Smith* [1997] that is available in CRTM. This brings the M-O bias closer to zero and significantly reduces its amplitude. The improvement is largest at low water vapors and smallest at large water vapors.

[29] Final CRTM implementation is shown in Figure 2c (including using a more appropriate SST as input to CRTM discussed in section 4.4 below). The M-O bias is close to zero at medium-to-large water vapors but it progressively increases toward low water vapors. (This dependence corroborates well with the zonal trends (shown in Figure 8 in section 5.1) and SST dependence of the M-O bias (not shown).) At least part of this high M-O bias may be due to the effect of SST on emissivity [Newman *et al.*, 2005], which has not been taken into account in the Wu-Smith emissivity model. According to Newman *et al.* [2005], including SST dependence would decrease emissivity at low temperatures and reduce the modeled surface BTs by several tenths of a Kelvin in AVHRR Ch5 spectral interval. Work is currently underway with the CRTM Team to improve the emissivity modeling for SST.

[30] Figure 3, similar in its structure to Figure 2, shows angular dependence of the M-O bias in Ch3B. The strong view-angle-dependent biases seen in Figure 3a for a black surface emissivity model are largely removed if a CRTM emissivity model is used instead (Figure 3b).

4.4. Using Reynolds Instead of NCEP SST

[31] The global (1°)² resolution SST field in the initial implementation of ACSPO was specified from the GFS

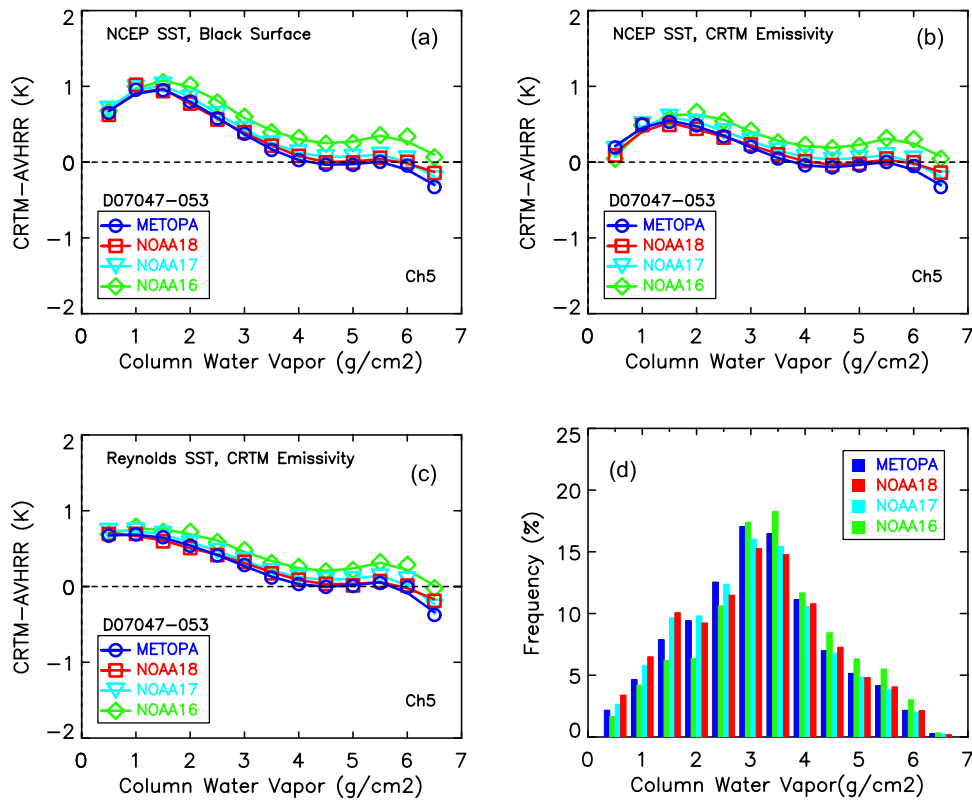


Figure 2. Same as in Figure 1 but for different parameters as CRTM input. (a) Black surface and NCEP SST, (b) CRTM emissivity and NCEP SST, (c) CRTM emissivity and Reynolds SST, and (d) corresponding histogram of W. Global data are for four platforms for 1 week from 16 to 22 February 2007.

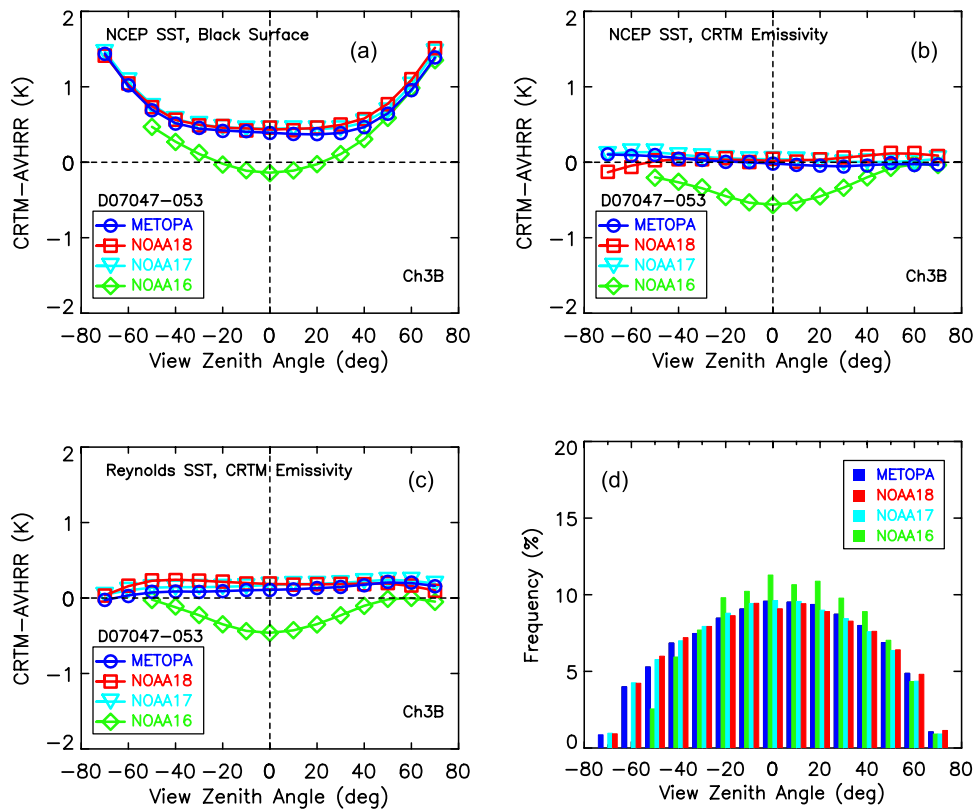


Figure 3. Same as in Figure 2 but as a function of view zenith angle for Ch3B. Data binned at $\Delta\theta = 10^\circ$.

parameter called “surface temperature,” which presumably comes from *Reynolds et al.*'s [2002] weekly v.2 SST over ocean and from land surface temperature over land. In ACSPO v.1, $(1^\circ)^2$ SST data are used as input to CRTM and then interpolated to match the satellite pixel. Whether a gridded value came from a land or sea pixel could be, in principle, determined by the land-sea mask. However, we have chosen to implement an optional additional input of *Reynolds et al.*'s [2002] weekly v.2 SST in ACSPO and directly compare the two results.

[32] Figures 2c and 3c show that using weekly v.2 Reynolds SST in place of NCEP SST has little effect on the M-O bias. The only exception is in Figure 2c at the low end of water vapor content ($<1.5\text{g/cm}^2$), where the M-O bias increases. To gain insight into this relapse, global maps of the M-O biases are shown in the top two panels of Figure 4 for NOAA-18 Ch3B, Figure 4a corresponding to Reynolds SST and Figure 4b to NCEP SST as input to CRTM. The most striking difference is in the coastal areas, where the M-O bias is unrealistically low in the case of NCEP SST, and its variability (not shown) is unrealistically high. Additional analyses have shown that the GFS column water vapor content and wind speed are also biased low in the coastal areas. If those areas are removed from the analyses, then the water vapor and wind speed dependencies of the M-O biases calculated with Reynolds weekly v.2 and GFS SST inputs look much closer (not shown; see also discussion below in section 4.6). Interestingly, the differences between the NCEP and Reynolds weekly v.2 SSTs are not only limited to the coastal areas, as attested by Figure 4c. These observations have been reported to the NCEP GFS Team. As of the time of this writing, it remains unknown to us what causes the difference between the NCEP and Reynolds SSTs in the open ocean.

4.5. Global Histograms of the M-O Bias

[33] Figure 5 systematically compares the M-O biases for all bands and platforms, when NCEP and Reynolds SSTs are used as input to CRTM. Using Reynolds SST increases the global M-O biases by $\sim 0.1\text{K}$, in all AVHRR bands, bringing them to $\sim +0.2\text{K}$ in Ch3b and $\sim +0.3\dots+0.4\text{K}$ in Ch4 and Ch5. Increased bias may not necessarily be “bad news” in this particular case, as it leaves a wider margin for the future incorporation of aerosols in the RTM, adjusting SST for diurnal cycle and using skin SST instead of current bulk. Also, we anticipate that the ongoing improvements in ACSPO nighttime clear-sky mask may bring the “O” up, thus further reducing the M-O bias.

[34] For SST analyses, it is critically important that the M-O biases in different bands are spectrally consistent. The fact that the margin is smallest in Ch3B, which is most sensitive to errors in SST and to aerosols, suggests that CRTM may need band-specific adjustments to its spectroscopy to simultaneously reconcile all three AVHRR bands.

[35] The analyses thus far have concentrated on the global mean M-O bias. Another important measure of CRTM-AVHRR consistency is its standard deviation (Stddev). Figure 5 shows that Stddevs become consistently smaller when Reynolds SST is used, for all bands and platforms. The difference is very significant and equivalent to cutting the M-O variance in half. For instance, in MetOp-A Ch3B, the balance is $(0.79\text{K})^2 - (0.56\text{K})^2 = (0.56\text{K})^2$. The decreased

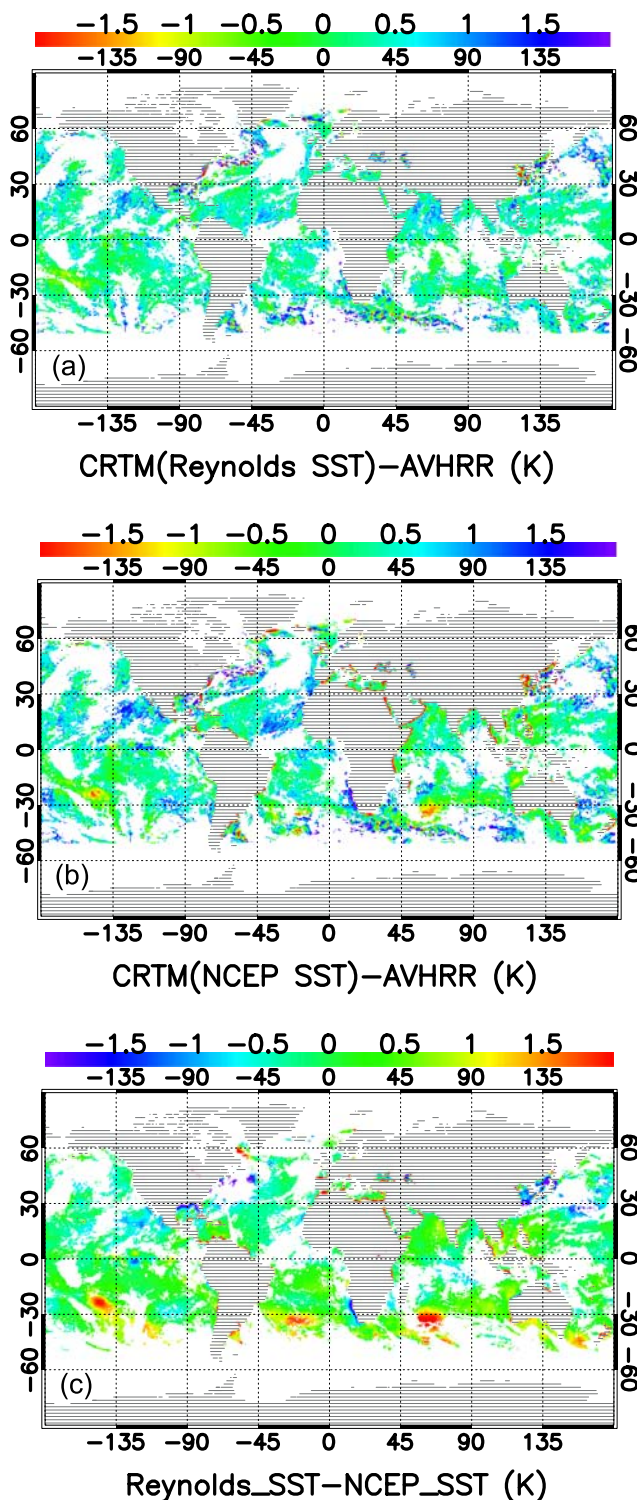


Figure 4. Global distribution of the M-O bias in NOAA-18-Ch3B, and corresponding Reynolds - NCEP SST differences for 1 day: 18 February 2007. (a) Reynolds SST, (b) NCEP SST used as input to CRTM, and (c) Reynolds minus NCEP SST. Note red contouring around the coastal lines in Figures 4b and 4c.

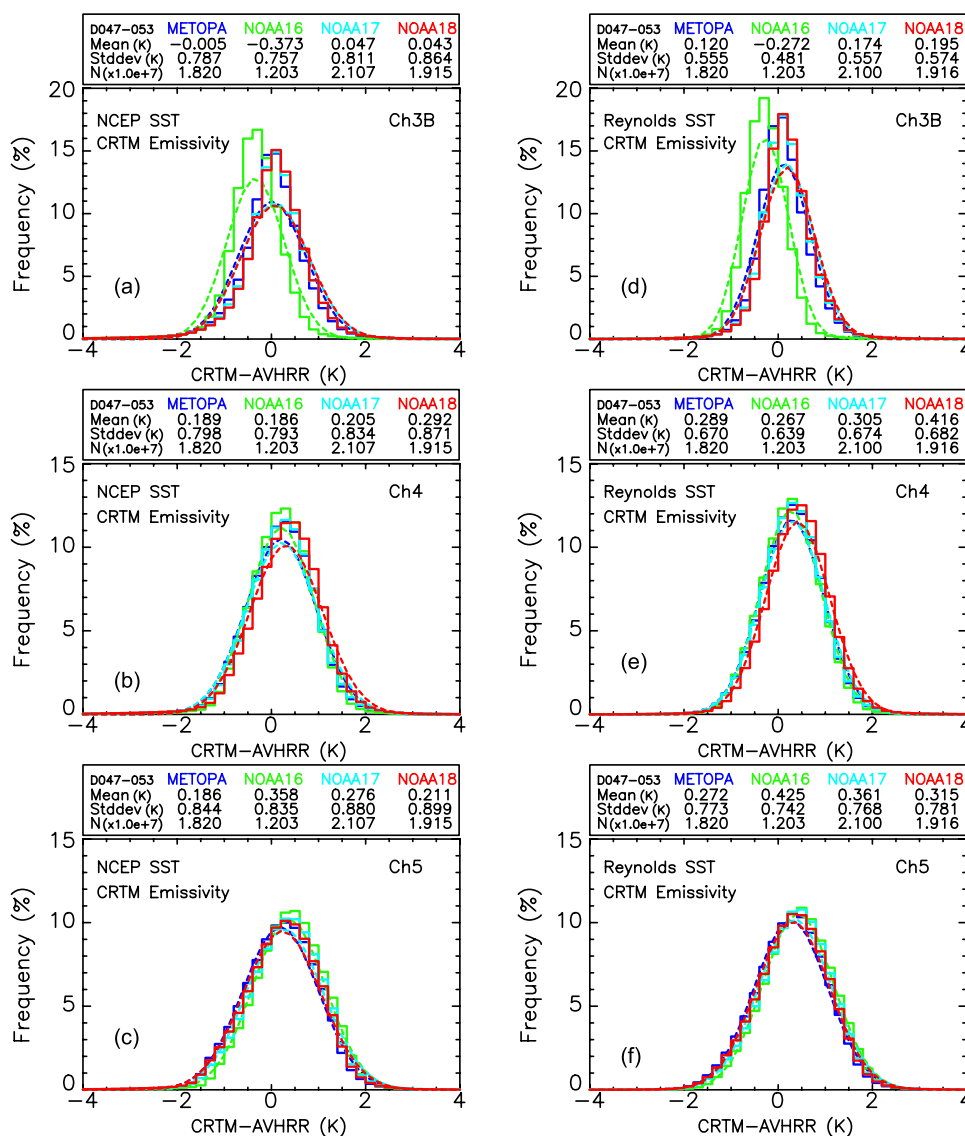


Figure 5. Histograms of the M-O bias for 1 week of global data from 16 to 22 February 2007. (a, b, c) NCEP SST and (d, e, f) Reynolds SST are used as input to CRTM. For Reynolds SST, all histograms are consistently narrower (Std Dev smaller) than for NCEP SST.

Stddev provides strong evidence that Reynolds SST is a superior predictor for the CRTM, compared to GFS SST.

[36] Cross-platform consistency is generally within 0.1K in all bands, indicating that the sensor calibrations and spectral response functions are largely consistent across four sensors. The only glaring exception is NOAA16 Ch3B. In a similar validation study of MODTRAN4.2 [Dash and Ignatov, 2008], the same anomaly was observed and thought to be due to a possible shift of its spectral response function. This atypical NOAA16 Ch3B result will be shown in the remainder of this paper but will not be discussed any further. On the other hand, the MetOp-A Ch3B, which was out-of-family in MODTRAN analyses, is now in-family, which is consistent with similar analyses by Merchant et al. [2008]. As of the time of this writing, the reason for this inconsistency is not clear to us. Analyses of the NOAA-16 and MetOp-A anomalies continue and their results will be reported elsewhere.

4.6. Using Skin Instead of Bulk SST and the Possible Effects of Aerosols

[37] Radiance measured by satellite sensor is sensitive to skin SST, whereas Reynolds weekly v.2 SST is tuned against in situ SSTs and, therefore, is a bulk SST product. In absence of diurnal thermocline at night, Donlon et al. [2002] suggest an empirical bulk-to-skin SST conversion using a wind speed-dependent parameterization of the form $T_{\text{skin}} = T_{\text{bulk}} - [0.14 + 0.30 \times \exp(-V/3.7)]$, where V is the near-surface wind speed. Skin-bulk difference may offset some of the warm M-O biases observed in Figure 5 ($\sim +0.2\text{K}$ in Ch3B and $\sim +0.3\text{...}+0.4\text{K}$ in Ch4 and Ch5).

[38] The amplitude of the wind speed dependence in Figure 6c (corresponding to skin SST) slightly increases from Figure 6b (corresponding to bulk SST) because the bulk-to-skin conversion suppresses the low wind speed domain most and affects the large wind speed domain least.

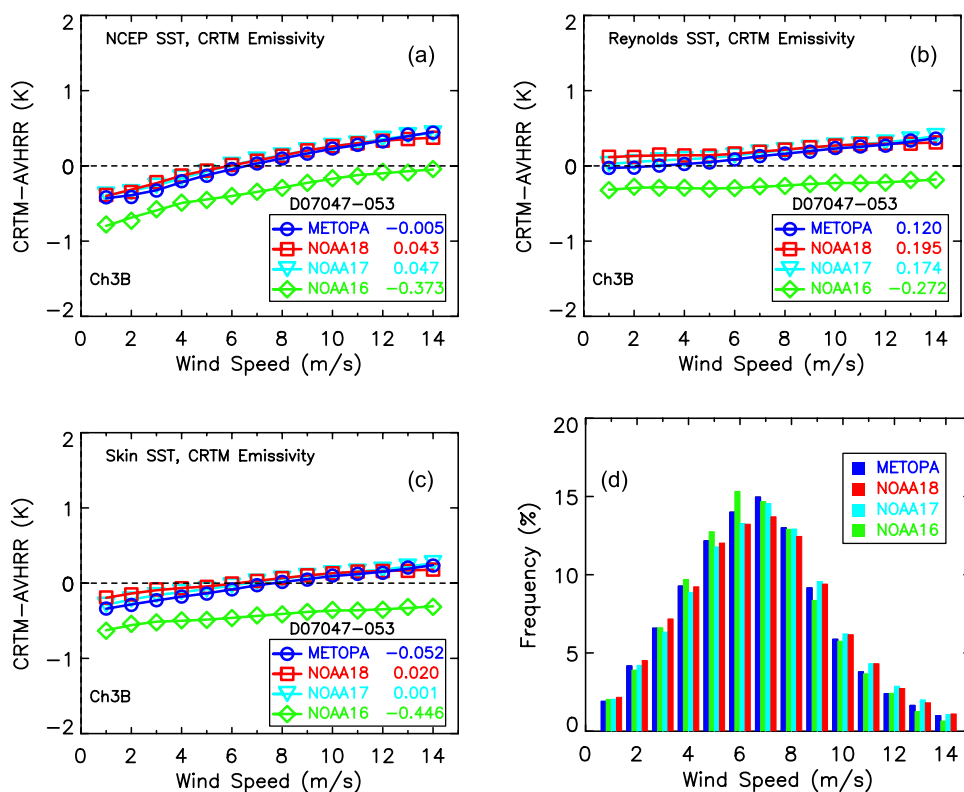


Figure 6. The M-O bias in Ch3B as a function of wind speed for 1 week of global data from 9 to 15 June 2007 for different SSTs as CRTM input. (a) NCEP SST, (b) Reynolds SST, (c) Skin SST, and (d) corresponding histogram of wind speed. Data binned at $\Delta V = 1$ m/s. The skin SST is obtained from Reynolds bulk SST by applying a wind speed-dependent correction by *Donlon et al.* [2002].

The shape of the dependence may be a complex combination of large-scale correlations between water vapor, SST, and wind speed, which in turn all have pronounced zonal distributions. This shape is not analyzed here.

[39] As expected, the bulk-to-skin conversion reduces the M-O bias and brings it closer to zero while keeping slightly positive. The reduction is ~ 0.17 K in Ch3B and somewhat smaller in Ch4 and Ch5 (not shown), owing to a more opaque atmospheric transmission in these bands. On the basis of some prior MODTRAN analyses, including background maritime tropospheric aerosols may account for another 0.1–0.2K, depending upon band [e.g., *Dash and Ignatov, 2008*]. Margins in Ch4 and Ch5 are about right for that correction, whereas Ch3B would be overcorrected if aerosols are included. Adjustments to the daily mean Reynolds SST to account for diurnal cycle may contribute another several tenths of a Kelvin offset. The CRTM thus appears to more accurately represent AVHRR data in the longwave IR window, whereas in the shortwave window, it may be slightly underestimated. There is also some evidence that Ch3B may be less sensitive to the Saharan dust and to the aged volcanic stratospheric aerosols than Ch4 and Ch5 [*Merchant et al., 1999, 2006*].

[40] Figure 6a also shows wind speed dependence of the M-O bias in case of NCEP SST input. The amplitude of the effect is about twice as large as in the case of Reynolds SST shown in Figure 6b. As discussed in section 4.4 above, this result is due to the fact that the GFS SST and wind speed

fields are both biased in the coastal areas and that these biases are correlated.

4.7. CRTM Settings Adopted in ACSPO Version 1

[41] On the basis of the sensitivity analyses in this section, ACSPO v.1 is set to use a consistent treatment of finite layers in NCEP/GFS atmospheric profiles, CRTM emissivity model, and Reynolds weekly v.2 SST instead of NCEP SST as input to CRTM in ACSPO v.1.

[42] Using daily Reynolds SST [*Reynolds et al., 2007*] is being evaluated for the future versions of ACSPO. Converting bulk to skin SST using GFS near-surface wind speed, and adjusting it for the effect of diurnal cycle (e.g., using climatological data similar to those of *Kennedy et al. [2007]*), are also being considered.

5. M-O Bias Distribution in Space and Time

[43] This section evaluates geographical distribution of the M-O bias in the ACSPO v.1 product using one day and checks for temporal stability using 1 week of global data.

5.1. Geographical Distribution of the M-O Bias

[44] Figure 7 shows global distribution of the M-O biases in three bands of MetOp-A on 18 February 2007, and Figure 8 shows their zonal dependence and the corresponding histograms. Biases are smallest in the tropics of the Southern Hemisphere (0° – 30° S) and increase toward higher latitudes.

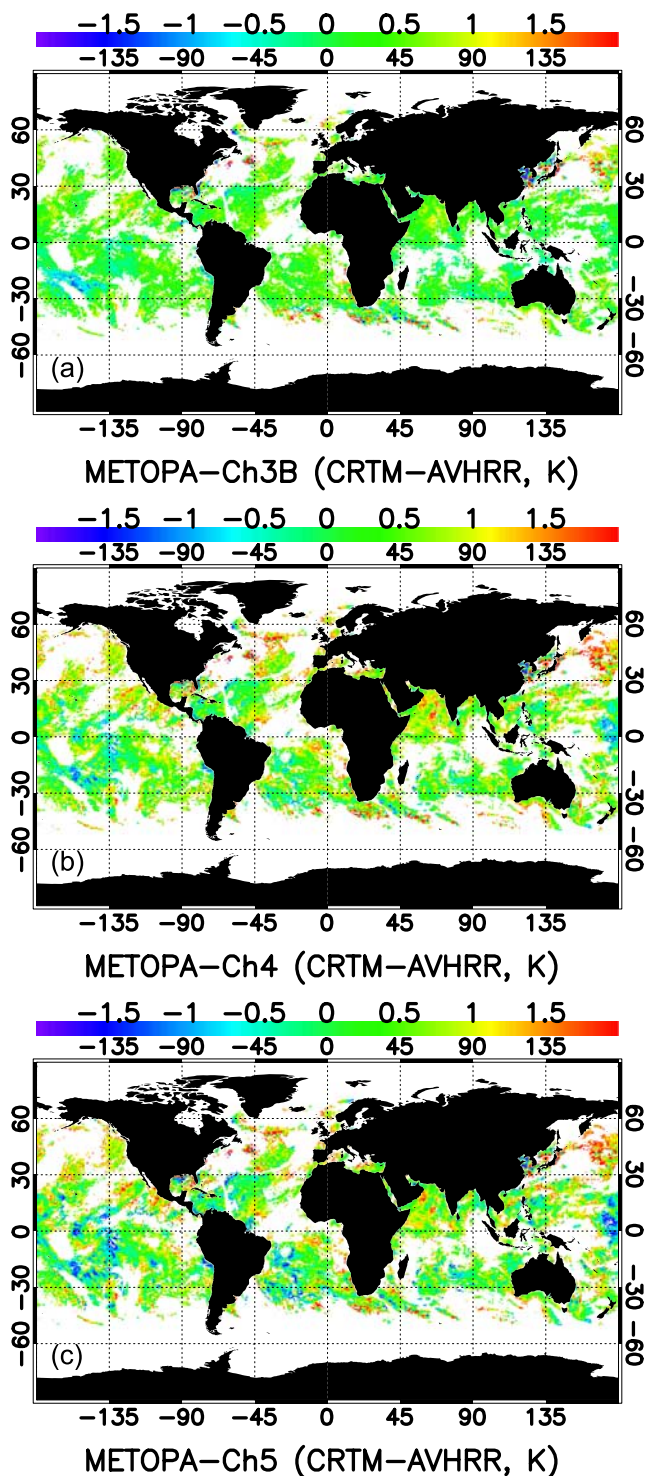


Figure 7. Global distribution of M-O biases in three AVHRR bands of MetOp-A on 18 February 2007.

Cross-platform consistency remains good in all three bands of all three platforms, in the full latitudinal range.

[45] These trends are likely due to the specifics of the zonal distributions of different geophysical factors such as ambient cloud, water vapor, and wind speed (see Figures 2 and 6, discussed earlier, and Figure 10 in section 6). Note that bias in the Northern Hemisphere is larger than in the Southern

Hemisphere. *Merchant et al.* [2008] attribute this asymmetry to differences in aerosol loading between the hemispheres. Future work will be aimed at minimizing artificial dependencies of the M-O bias on these factors, which should also minimize the M-O bias and improve its geographical uniformity.

5.2. Time Series of the M-O Bias

[46] Figure 9 shows a time series of the mean bias and its standard deviation for individual days from 16 to 22 February 2007. The empirical data points show less noise in Ch3B than in Ch4 and Ch5. A more stable CRTM performance in Ch3B is likely due to the smaller water vapor absorption in this band compared to the other two bands. The biases are $\sim 0.2\text{K}$ in Ch3B and $\sim 0.3\text{--}0.4\text{K}$ in Ch4 and Ch5, and respective Stddevs are 0.6, 0.7, and 0.8K. These numbers are very similar to the respective cumulative weekly statistics shown in Figure 5. All statistics thus appear stable and reproducible from day to day, at least during the week analyzed here.

[47] Work is currently underway to establish long-term monitoring of the M-O biases similarly to how they are monitored by the Numerical Weather Prediction Centers [e.g., *Garand*, 2003; *Köpken et al.*, 2004; *Munro et al.*, 2004] and to publish results on the Web at www.star.nesdis.noaa.gov/sod/sst/micros/ in near-real time. Such monitoring is helpful to evaluate the long-term performance of CRTM, and also assess stability and cross-platform consistency of the clear-sky BTs over oceans.

6. Effect of Ambient Clear-Sky Environment on the M-O Bias

[48] A part of the warm M-O bias may come from a cold bias in the “O,” which could be due to the contribution from the ambient and/or residual cloud in AVHRR BTs. The vicinity of cloud may be surrounded by elevated aerosols and water vapor (the so-called “cloud halos”), which may also be favored for cloud formation. Such transient states are difficult to detect using a threshold-based ACSPO clear-sky mask and they are not modeled in CRTM (see discussion and references in work by *Dash and Ignatov* [2008]).

[49] Here, we attempt to quantify the effect of ambient and/or residual cloud on the M-O bias, with the objective to validate the “true” performance of the CRTM in which this effect was not modeled. For that, the M-O dependencies are fit as a function of the number of clear-sky ocean pixels surrounding the central pixel (NCSOP [cf. e.g., *Trigo and Viterbo*, 2003; *Köpken et al.*, 2004; *Munro et al.*, 2004]) within a 25-by-25 sliding window. This size of the window was chosen empirically to approximately match the 1° latitude-by-longitude area used by *Dash and Ignatov* [2008]. Note that some 25-by-25 windows may include coast, land, ice, or some invalid pixels. No attempt was made here to differentiate between those boundary pixels and cloud. For the analyses in this section, only NCSOP was used as a predictor.

[50] Figure 10 shows the effect of NCSOP on the mean M-O biases in three channels of four sensors and corresponding NCSOP histograms. An exponential model was selected to approximate these curves as follows:

$$\Delta T = A + B^* \exp(-C^* \text{NCSOP}). \quad (3)$$

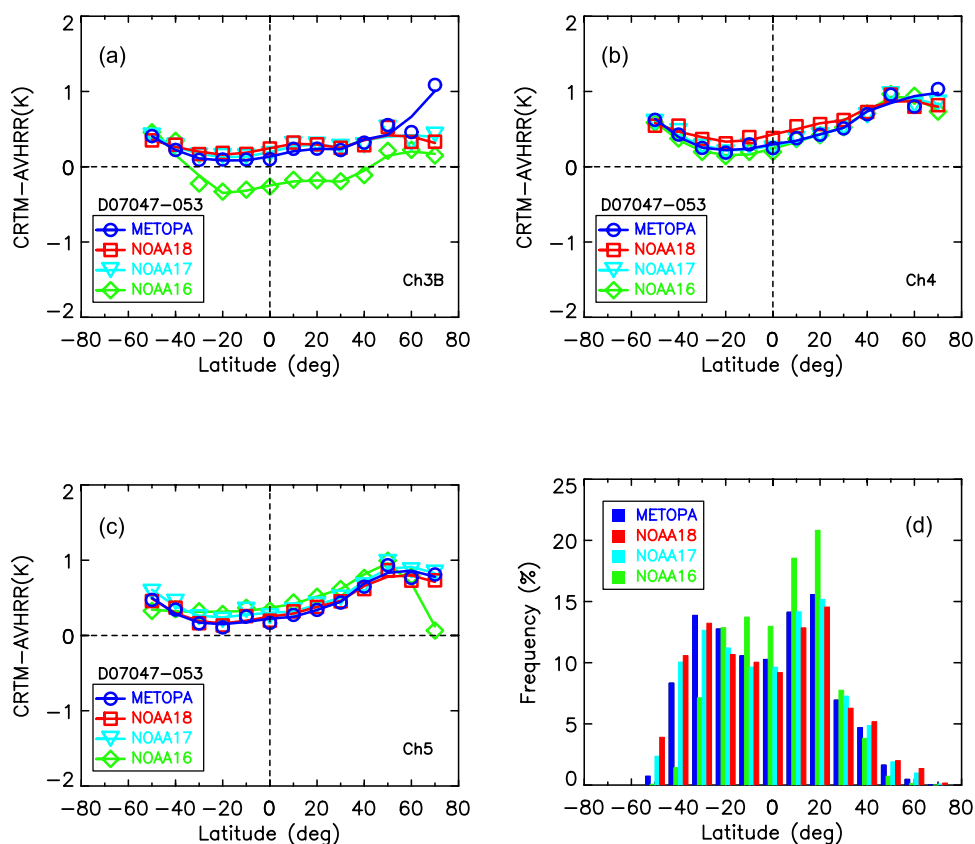


Figure 8. Zonal distribution of the M-O bias and histogram of latitude. Data binned at $\Delta\phi = 10^\circ$. Global data are for 1 week from 16 to 22 February 2007.

The fit equation approximates the M-O bias data well. The fit parameters, A , B , and C , are also listed in Figure 10. Two asymptotic regimes are of interest: (1) confident clear sky (NCSOP $\rightarrow \infty$), described by the parameter A , and (2) entire cloud (NCSOP $\rightarrow 0$), described by the $(A + B)$ aggregate, respectively. Parameters B and C represent the amplitude of the M-O bias and its dropoff rate with NCSOP, respectively.

[51] From the entire cloud to confident clear sky, the mean M-O biases change significantly. The amplitude (coefficient B) is $\sim 0.5\text{K}$ in Ch3B, $\sim 0.6\text{--}0.7\text{K}$ in Ch4, and $\sim 0.7\text{--}0.8\text{K}$ in Ch5. The curves drop off sharper in Ch4 and Ch5 than in Ch3B (coefficient C). These observations may be helpful to guide future improvements to ACSPO clear-sky mask.

[52] The curves stabilize themselves at large enough NCSOP (suggesting that a large fraction of the ACSPO data is affected by ambient and residual cloud) and approach an asymptotic clear-sky value characterized by the parameter A . The A parameter is expected to best characterize the “true” accuracy of CRTM, which currently does not model the effects of ambient and residual cloud. The asymptotic M-O biases are $\sim 0\text{K}$ in Ch3B and $\sim 0.1\text{--}0.2\text{K}$ in Ch4 and Ch5. Recall that aerosols were not included in CRTM and bulk SST is used, which was also not corrected for the effects of diurnal cycle. Once these factors are included, the M-O biases will likely become negative suggesting that absorption in

CRTM is probably somewhat overestimated. Analyses are underway to quantify these effects more accurately.

7. Discussion and Conclusions

[53] CRTM was integrated into ACSPO, where it is used in conjunction with NCEP GFS upper air and Reynolds weekly v.2 SST fields to predict TOA AVHRR BTs. With careful treatment of input data in the CRTM, an accurate implementation was obtained and the M-O biases were minimized.

[54] Overall, CRTM is an accurate model that closely reproduces AVHRR BTs in Ch3B, Ch4, and Ch5 for NOAA-16–18 and MetOp-A. The CRTM M-O biases appear much smaller and more spectrally consistent than those of MODTRAN4.2 [cf. *Merchant and Le Borgne*, 2004; *Dash and Ignatov*, 2008]. The M-O biases appear stable in time and show good cross-platform consistency in all cases except for Ch3B on NOAA-16, which shows an anomalous behavior. Note that MetOp-A Ch3B, which was out of family in the MODTRAN-AVHRR validation analysis by *Dash and Ignatov* [2008], is now in-family and shows no apparent anomaly [cf. *Merchant et al.*, 2008]. These NOAA-16 irregularities and MetOp-A inconsistencies are currently being investigated.

[55] The M-O bias was evaluated as a function of main factors affecting the M-O bias and accuracy of SST retrievals. Residual dependencies on the column water vapor, wind

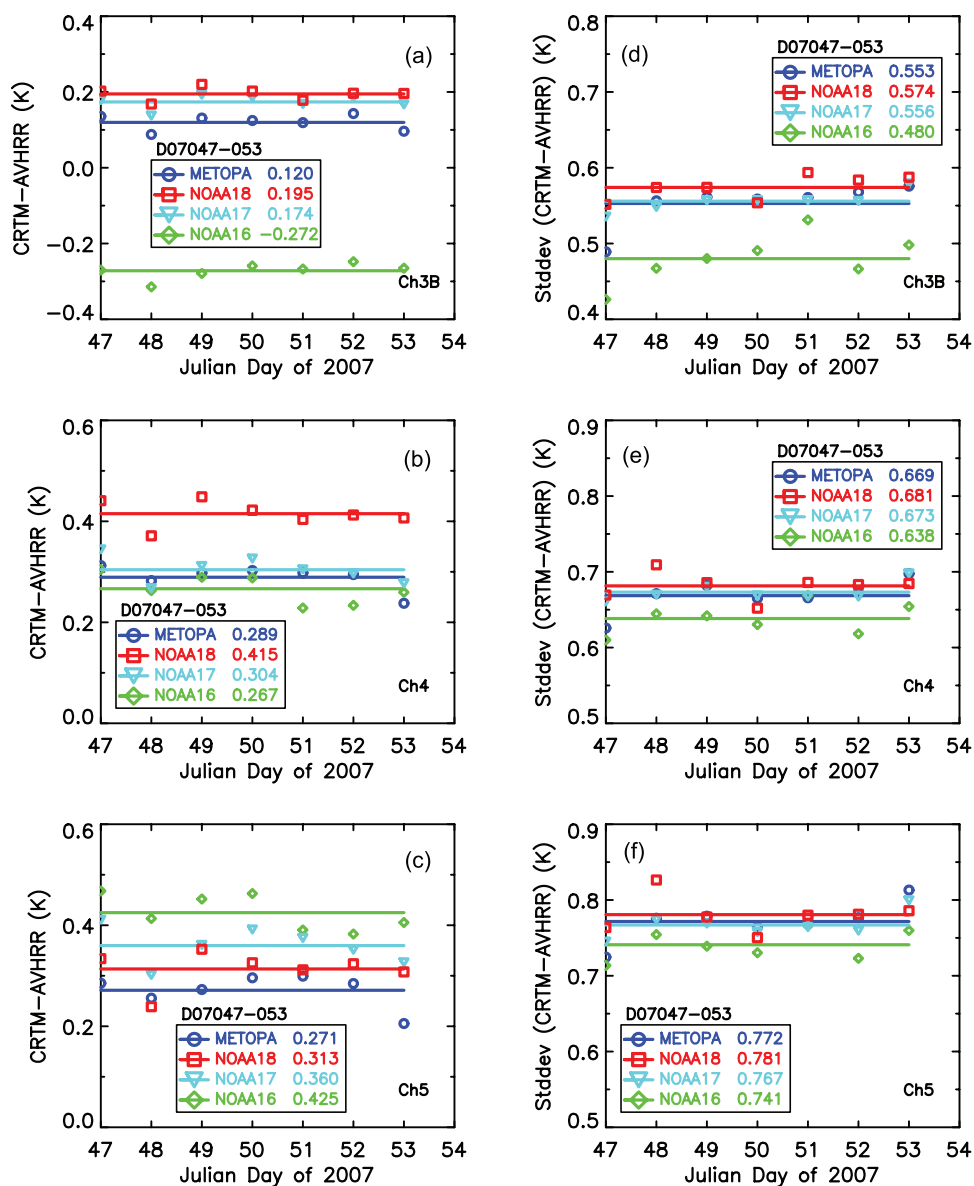


Figure 9. Time series of the (a, b, c) mean M-O bias and (d, e, f) standard deviation for 1 week of global data from 16 to 22 February 2007.

speed, sensor zenith angle, latitude, and ambient clear-sky environment have been detected. This is not fully unexpected because the validation was performed in the full global retrieval domain, and no data were withheld from analyses. Also, no bias correction was attempted for observed BTs, in contrast to customary practice in numerical assimilation of satellite data [e.g., *Uddstrom and McMillin*, 1994; *Garand*, 2003; *Köpken et al.*, 2004; *Munro et al.*, 2004; *Merchant et al.*, 2008].

[56] The global mean M-O biases are on the order of ~ 0.2 and $\sim 0.35\text{K}$ in Ch3B and Ch4/5, respectively. If asymptotic clear-sky conditions are considered, then these biases are reduced to only 0 to 0.2K . Including aerosols, using skin SST, and correcting it for the effects of diurnal cycle will likely make the M-O biases negative in all AVHRR bands. Analyses continue to incorporate all these factors and better quantify the “true” M-O bias.

[57] The current analyses suggest that the CRTM implementation in ACSPO in conjunction with GFS upper air and Reynolds SST inputs is already accurate enough to be used in the improved ACSPO cloud mask [*Petrenko et al.*, 2008; *Dybbroe et al.*, 2005; *Merchant et al.*, 2005] and physical SST retrievals [e.g., *Merchant et al.*, 2008]. To that end, tangent-linear, adjoint, and K-Matrix models that are critically important for the inversions are now available in CRTM [*Han et al.*, 2006]. Adding aerosol and reflected solar radiation in the CRTM will be required for accurate physical SST retrievals, especially during daytime. We also consider testing the CRTM with the data from other numerical weather prediction (NWP) atmospheric models, such as the ECMWF data and NCEP Reanalysis. Daily Reynolds SST [*Reynolds et al.*, 2007] is also being explored. We also plan to extend our validation analyses to the daytime data. Each improvement in

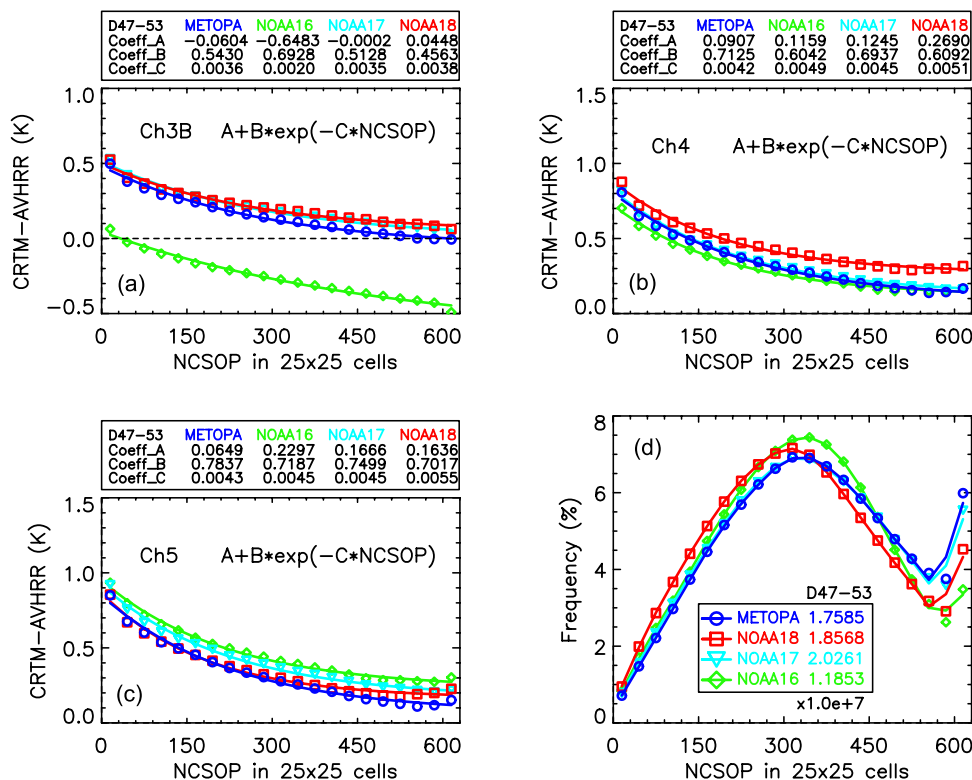


Figure 10. The M-O biases as a function of the number of clear-sky ocean pixels (NCSOP) within 25×25 cells. Data were binned at $\Delta N = 30$. One week of global data from 16 to 22 February 2007.

the forward model will be quantitatively evaluated using the methodology described in this paper.

[58] The developed system will be applied to the MSG/SEVIRI radiances, to prepare for the GOES-R/ABI. Resources permitting, it will also be tested with MODIS radiances, to get ready for processing the Visible and Infrared Imaging Radiometer Suite (VIIRS) onboard the National Polar Orbiting Environmental Satellite System (NPOESS).

[59] **Acknowledgments.** This work is conducted under the Algorithm Working Group funded by the GOES-R Program Office. X.-M. Liang also acknowledges the CIRA visiting scientist fellowship. CRTM is provided by the NESDIS Joint Center for Satellite Data Assimilation (JCSDA). Thanks go to Andrew Heidinger, Prasanjit Dash, Boris Petrenko, Yong Han, Quanhua Liu, Yong Chen, Paul Van Delst, and David Groff of NOAA/NESDIS for advice and help, and to two anonymous reviewers of this manuscript for careful reviews and useful recommendations. The views, opinions, and findings contained in this report are those of the authors and should not be construed as an official NOAA or U.S. Government position, policy, or decision.

References

- Cao, C., M. Weinreb, and J. Sullivan (2001), Solar contamination effects on the infrared channels of the advanced very high resolution radiometer, *J. Geophys. Res.*, *106*, 33,463–33,469, doi:10.1029/2001JD001051.
- Clough, S. A., M. W. Shephard, E. J. Mlawer, J. S. Delamere, M. J. Iacono, K. Cady-Pereira, S. Boukabara, and P. D. Brown (2005), Atmospheric radiative transfer modeling: A summary of AER codes, *J. Quant. Spectrosc. Radiat. Transfer*, *91*, 233–244.
- Dash, P., and A. Ignatov (2008), Validation of clear-sky radiances over oceans simulated with MODTRAN4.2 and global NCEP GDAS fields against nighttime NOAA15–18 and MetOp-A AVHRRs data, *Remote Sens. Environ.*, *112*, 3012–3029, doi:10.1016/j.rse.2008.02.013.
- Donlon, C. J., P. J. Minnett, T. J. Gentemann, I. J. Barton, B. Ward, and M. J. Murray (2002), Toward improved validation of satellite surface skin temperature measurements for climate research, *J. Clim.*, *15*, 353–369, doi:10.1175/1520-0442(2002)015<0353:TIVOSS>2.0.CO;2.

- Dybbroe, A., K. G. Karlsson, and A. Thoss (2005), NWCSAF AVHRR cloud detection and analysis using dynamic thresholds and radiative transfer modeling, Part 1: Algorithm description, *J. Appl. Meteorol.*, *44*, 39–54, doi:10.1175/JAM-2188.1.
- Flatau, P. J., R. L. Walko, and W. R. Cotton (1992), Polynomial fits to saturation vapor pressure, *J. Appl. Meteorol.*, *31*, 1507–1513, doi:10.1175/1520-0450(1992)031<1507:PFTSVP>2.0.CO;2.
- Garand, L. (2003), Toward an integrated land-ocean surface skin temperature analysis from the variational assimilation of infrared radiances, *J. Appl. Meteorol.*, *42*, 570–583, doi:10.1175/1520-0450(2003)042<0570:TALSS>2.0.CO;2.
- Goff, J. A., and S. Gratch (1946), Low-pressure properties of water from -160 to 212°F , *Trans. Am. Soc. Heat. Ventil. Eng.*, *52*, 95–122.
- Guildner, L., D. P. Johnson, and F. E. Jones (1976), Vapor pressure of water at its triple point, *J. Res. Natl. Bur. Stand. U. S., Sect. A*, *80*, 505–521.
- Han, Y., P. van Delst, Q. Liu, F. Weng, B. Yan, R. Treadon, and J. Derber (2006), JCSDA Community Radiative Transfer Model (CRTM)–Version 1, *NOAA Tech. Rep. NESDIS 122*, 33 pp., NOAA, Silver Spring, Md.
- Ignatov, A., J. Sapper, I. Laszlo, N. Nalli, A. Harris, W. Pichel, A. E. Strong, E. Bayler, X. Li, and E. Maturi (2004), Global operational sea surface temperature and aerosol products from AVHRR: Current status, diagnostics, and potential enhancements, paper presented at 13th AMS Conference on Satellite Oceanography and Meteorology, Am. Meteorol. Soc., Norfolk, Va.
- Kennedy, J. J., P. Brohan, and S. F. B. Tett (2007), A global climatology of the diurnal variations in sea surface temperature and implications for MSU temperature trends, *Geophys. Res. Lett.*, *34*, L05712, doi:10.1029/2006GL028920.
- Kleespies, T. J., P. van Delst, L. M. McMillin, and J. Derber (2004), Atmospheric transmittance of an absorbing gas. 6. An OPTRAN status report and introduction to the NESDIS/NCEP Community Radiative Transfer Model, *Appl. Opt.*, *43*, 3103–3109, doi:10.1364/AO.43.003103.
- Köpken, C., G. Kelly, and J.-N. Thépaut (2004), Assimilation of Meteosat radiance data within the 4D-Var system at ECMWF: Assimilation experiments and forecast impact, *Q. J. R. Meteorol. Soc.*, *130*, 2277–2292, doi:10.1256/qj.02.230.
- Masuda, K. (2006), Infrared sea surface emissivity including multiple reflection effect for isotropic Gaussian slope distribution model, *Remote Sens. Environ.*, *103*, 488–496, doi:10.1016/j.rse.2006.04.011.
- McClain, E. P., W. G. Pichel, and C. C. Walton (1985), Comparative performance of AVHRR-based multichannel sea surface temperatures, *J. Geophys. Res.*, *90*, 11,587–11,601, doi:10.1029/JC090iC06p11587.

- McMillin, L. M., X. Xiong, Y. Han, T. J. Kleespies, and P. Van Delst (2006), Atmospheric transmittance of an absorbing gas. 7. Further improvements to the OPTRAN approach, *Appl. Opt.*, *45*, 2028–2034, doi:10.1364/AO.45.002028.
- Merchant, C. J., and P. Le Borgne (2004), Retrieval of sea surface temperature from space, based on modeling of infrared radiative transfer: Capabilities and limitations, *J. Atmos. Oceanic Technol.*, *21*, 1734–1746, doi:10.1175/JTECH1667.1.
- Merchant, C. J., A. R. Harris, M. J. Murray, and A. M. Závody (1999), Toward the elimination of bias in satellite retrievals of sea surface temperature: 1. Theory, modeling and interalgorithm comparison, *J. Geophys. Res.*, *104*, 23,565–23,578, doi:10.1029/1999JC900105.
- Merchant, C. J., A. R. Harris, E. Maturi, and S. MacCallum (2005), Probabilistic physically based cloud screening of satellite infra-red imagery for operational sea surface temperature retrieval, *Q. J. R. Meteorol. Soc.*, *131*, 2735–2755, doi:10.1256/qj.05.15.
- Merchant, C. J., O. Embury, P. Le Borgne, and B. Bellec (2006), Saharan dust in nighttime thermal imagery: Detection and reduction of related biases in retrieved sea surface temperature, *Remote Sens. Environ.*, *104*, 15–30, doi:10.1016/j.rse.2006.03.007.
- Merchant, C. J., P. Le Borgne, A. Marsouin, and H. Roquet (2008), Optimal estimation of sea surface temperature from split-window observations, *Remote Sens. Environ.*, *112*, 2469–2484, doi:10.1016/j.rse.2007.11.011.
- Munro, R., C. Köpken, G. Kelly, J.-N. Théapaut, and R. Saunders (2004), Assimilation of Meteosat radiance data within the 4D-Var system at ECMWF: Data quality monitoring, bias correction, and single-cycle experiments, *Q. J. R. Meteorol. Soc.*, *130*, 2293–2313, doi:10.1256/qj.02.229.
- Newman, S. M., J. A. Smith, M. D. Glew, S. M. Rogers, and J. P. Taylor (2005), Temperature and salinity dependence of sea surface emissivity in the thermal infrared, *Q. J. R. Meteorol. Soc.*, *131*, 2539–2557, doi:10.1256/qj.04.150.
- Petrenko, B., A. Heidinger, A. Ignatov, and Y. Kihai (2008), Clear-sky mask for the AVHRR Clear-Sky Processor for Oceans, paper presented at Ocean Sciences Meeting, Am. Soc. of Limnol. and Oceanogr., Orlando, Fla. (http://www.star.nesdis.noaa.gov/smcd/emb/aerosol/ignatov/conf/2008-AGU-OSM-PetrenkoEtAl_ACSPO_CSM_Poster.pdf)
- Reynolds, R. W., N. A. Rayner, T. M. Smith, D. C. Stokes, and W. Wang (2002), An improved in situ and satellite SST analysis for climate, *J. Clim.*, *15*, 1609–1625, doi:10.1175/1520-0442(2002)015<1609:AISAS>2.0.CO;2.
- Reynolds, R. W., T. M. Smith, C. Liu, D. B. Chelton, K. S. Casey, and M. G. Schlax (2007), Daily high-resolution blended analyses for sea surface temperature, *J. Clim.*, *20*, 5473–5496, doi:10.1175/2007JCLI1824.1.
- Rothman, L. S., et al. (2003), The HITRAN molecular spectroscopic database: Edition of 2000 including updates through 2001, *J. Quant. Spectrosc. Radiat. Transfer*, *82*, 5–44.
- Saunders, R., M. Matricardi, and P. Brunel (1999), An improved fast radiative transfer model for assimilation of satellite radiances observations, *Q. J. R. Meteorol. Soc.*, *125*, 1407–1425, doi:10.1256/smsqj.55614.
- Saunders, R., et al. (2007), A comparison of radiative transfer models for simulating Atmospheric Infrared Sounder (AIRS) radiance, *J. Geophys. Res.*, *112*, D01S90, doi:10.1029/2006JD007088.
- Sherlock, V. (1999), *ISEM-6: Infrared surface emissivity model for RTTOV-6*, *Forecast. Res. Tech. Rep.* 299, 17 pp., NWP Div., MetOffice, Exeter, U. K.
- Sherlock, V., A. Collard, S. Hannon, and R. Saunders (2003), The gas-tropod fast radiative transfer model for advanced infrared sounders and characterization of its errors for radiance assimilation, *J. Appl. Meteorol.*, *42*, 1731–1747, doi:10.1175/1520-0450(2003)042<1731:TGFRTM>2.0.CO;2.
- Trigo, I. F., and P. Viterbo (2003), Clear-sky window channel radiances: A comparison between observations and the ECMWF model, *J. Appl. Meteorol.*, *42*, 1463–1479, doi:10.1175/1520-0450(2003)042<1463:CWCRCAC>2.0.CO;2.
- Uddstrom, M. J., and L. M. McMillin (1994), System noise in the NESDIS TOVS forward model. Part 1: Specifications, *J. Appl. Meteorol.*, *33*, 919–938, doi:10.1175/1520-0450(1994)033<0919:SNITNT>2.0.CO;2.
- Walton, C. C., W. G. Pichel, J. F. Sapper, and D. A. May (1998), The development and operational applications of nonlinear algorithms for the measurement of sea surface temperatures with the NOAA polar-orbiting environmental satellites, *J. Geophys. Res.*, *103*, 27,999–28,012.
- Wan, Z., and J. Dozier (1996), A generalized split-window algorithm for retrieving land-surface temperature from space, *IEEE Trans. Geosci. Remote Sens.*, *34*, 892–905, doi:10.1109/36.508406.
- Watts, P. D., M. R. Allen, and T. J. Nightingale (1996), Wind speed effects on sea surface emission and reflection for the Along Track Scanning Radiometer, *J. Atmos. Oceanic Technol.*, *13*, 126–141, doi:10.1175/1520-0426(1996)013<0126:WSEOSS>2.0.CO;2.
- Wu, X., and W. L. Smith (1997), Emissivity of rough sea surface for 8–13 μ m: Modeling and verification, *Appl. Opt.*, *36*, 2609–2618, doi:10.1364/AO.36.002609.

A. Ignatov, Y. Kihai, and X.-M. Liang, Center for Satellite Application and Research, NESDIS, NOAA, WWB Room 603, 5200 Auth Road, Camp Springs, MD 20746, USA. (xingming.liang@noaa.gov)